Modeling study of radiation characteristics with different impurity species seeding in EAST

X. J. Liu, G. Z. Deng, L. Wang, S. C. Liu, L. Zhang, G. Q. Li, and X. Gao

Citation: Physics of Plasmas **24**, 122509 (2017);
View online: https://doi.org/10.1063/1.4997101
View Table of Contents: http://aip.scitation.org/toc/php/24/12
Published by the American Institute of Physics

Modeling study of radiation characteristics with different impurity species seeding in EAST

X. J. Liu,[1,a)] G. Z. Deng,[1,2] L. Wang,[1,3] S. C. Liu,[1] L. Zhang,[1] G. Q. Li,[1] and X. Gao[1,2]
[1]*Institute of Plasma Physics, Chinese Academy of Sciences, Hefei 230031, China*
[2]*University of Science and Technology of China, Hefei 230026, China*
[3]*School of Physics and Optoelectronic Technology, Dalian University of Technology, Dalian 116024, China*

(Received 21 July 2017; accepted 21 November 2017; published online 14 December 2017)

A critical issue for EAST and future tokamak machines such as ITER and China Fusion Engineering Testing Reactor is the handling of excessive heat load on the divertor target plates. As an effective means of actively reducing and controlling the power fluxes to the target plates, localized impurity (N, Ne, and Ar) gas puffing from the lower dome is investigated by using SOLPS5.0 for an L-mode discharge on EAST with double null configuration. The radiative efficiency and distribution of different impurities are compared. The effect of N, Ne, and Ar seeding on target power load, the power entering into scrape-off layer (SOL), P_{sep}, and their concentration in SOL along the poloidal length and edge effective ion charge number (Z_{eff}) which are closely related to core plasma performance are presented. The simulation results indicate that N, Ne, and Ar seeding can effectively reduce the peak heat load and electron temperature at divertor targets similarly. N seeding can reach the highest radiative loss fraction and both N and Ar strongly radiate power in the divertor region, while the radiative power inside the separatrix for Ar seeding is also significant. Ne radiates power mainly around the separatrix and X-point. Ne and Ar impurities' puffing results in a faster decrease of P_{sep} than N seeding case; the reduction of P_{sep} can eventually degrade the core performance of fusion plasma. Additionally, seeding with Ne has a totally larger concentration at the outer midplane and edge Z_{eff} than those in N and Ar seeding cases; it suggests that N and Ar impurities are more acceptable than Ne in terms of fuel dilution for this discharge. *Published by AIP Publishing*. https://doi.org/10.1063/1.4997101

I. INTRODUCTION

The mitigation of divertor heat flux is an active topic of investigation on present tokamaks. It is also a critical issue for EAST to explore a long pulse and high heating power operation.[1] This problem may become more crucial if carbon has to be avoided as a plasma facing material (PFC) for future reactors, like ITER and China Fusion Engineering Testing Reactor (CFETR),[2] due to its high co-deposition of tritium.[3] For future reactors, fueling particles and an acceptable level (i.e., low core fuel dilution) low-z intrinsic impurities (like Be) are not expected to decrease the power flux on the divertor to an acceptable level due to its low radiative loss rate. One promising approach is seeding impurity gases with a high radiative loss rate to enhance the radiation power with the dominant portion concentrated outside the last closed flux surface (LCFS), especially in the divertor region, and eventually to reduce the heat load on target plates. Divertor dominated radiation loss requires a high enrichment of impurities in the divertor region[4–7] and also a high radiative loss rate in the temperature range prevailed in divertor. This technique has been investigated on a number of tokamaks.[8–12] The experimental results on ALCATOR C-Mod demonstrate that regardless of the species of impurity, the confinement depends primarily on the net power across the separatrix, which suggests that applying impurity seeding is necessary to remove heat from the plasma outside the separatrix rather than inside of LCFS. The results on ALCATOR C-Mod,[8,9] ASDEX-Upgrade,[10] and JET[11] also illustrate that nitrogen is well suited and even better than other impurities like Ne and Ar to simultaneously control divertor heat load and to achieve good confinement due to N radiating power concentrated in the divertor region. In EAST, the recent modeling and experiments on Ar seeding in H-mode plasma show that Ar is effective to mitigate the heat load onto the divertor target and achieve partial detachment by radiating power in edge plasma region as well as the main plasma region.[12] However, the present measurement of radiation cannot make a well distinction in the vicinity of the X-point and around the separatrix due to the existence of uncertainty in the position of LCFS, so where the radiation dissipation occurs is not exactly clear. Otherwise, it is extremely difficult to keep all parameters the same with different impurity seeding in experiments to make an elaborate comparison since the tokamak plasma is highly complicated. In order to make a detailed comparison among N, Ne, and Ar for optimization of the species and puffing rate of impurity seeded, modeling analysis is necessary to understand well the radiative power distribution and their effect on heat load on divertor targets and core performance.

In this paper, we use the SOLPS5.0 code package[13] for the simulations of scrape-off layer (SOL) and divertor plasma. SOLPS mainly consists of two coupled codes: B2.5 is a fluid code that solves Braginskii-like equations for the

[a)]Email: julie1982@ipp.ac.cn

ions (D, C, He, N, Ne, Ar) and electrons. Eirene is a Monte Carlo code that describes kinetic neutrals.[14] Both codes are coupled via source terms of particle, momentum, and energy. As we know, the atomic physics model and database are significant in determining the plasma constituents and the interaction among them. Since ADAS (Atomic Data and Analysis Structure) database[15] is actively maintained and upgraded, the main atomic processes included in this work, for example, ionization, excitation, dissociation, charge exchange, and elastic collisions, are from ADAS database. The accuracy of the data is mostly considered to be about 10%–20%.

The divertor geometry of EAST and computational mesh used by SOLPS5.0 including the modeling setups are briefly described in Sec. II. Detailed modeling studies of radiation power balance in core and edge with N, Ne, and Ar seeding and their effects on the mitigation of divertor heat load and the power entering into SOL (P_{sep}) as well as their concentration in SOL region along the poloidal length and edge effective ion charge number (Z_{eff}) are presented and discussed in Sec. III. Finally, conclusions from the modeling results are given in Sec. IV.

II. SIMULATION PARAMETERS

A. Geometry and computational grid

A grid is constructed for double null shot 41383 at 4.5 s shown as Fig. 1 which is a typical double null configuration L-mode discharge with lower hybrid wave heating power $P_{in} \sim 2$ MW, the plasma current $Ip \sim 400$ kA, the toroidal field $B_t \approx 1.8$ T (reversed direction, it means $B \times \nabla B$ drift towards the lower X-point), and the line-averaged electron density $n_e \sim 4.0 \times 10^{19}\,m^{-3}$.

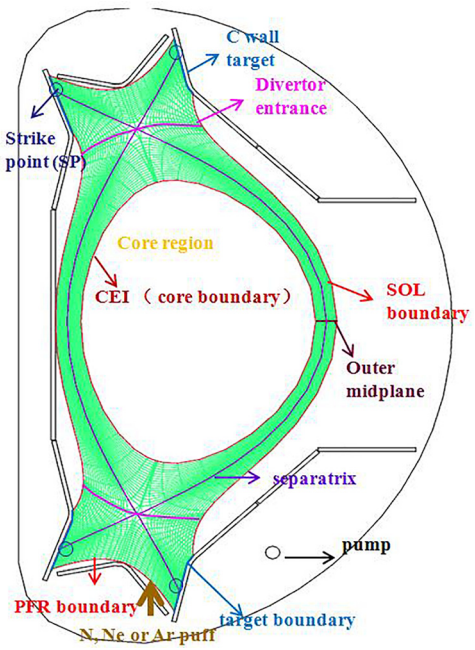

FIG. 1. The 2 D physical mesh for modeling. The impurity gas (N, Ne, and Ar) is injected from the lower dome and D_2 puffing for controlling the electron density at the outer midplane separatrix. The boundaries are pointed out with arrows.

The divertor PFCs are carbon and molybdenum (Mo) tiles for the main chamber wall for this shot. It should be noted that the upper divertor has been upgraded to ITER-like mono-block tungsten (W) since 2014,[21] and the lower divertor will further be replaced by mono-block tungsten (W) to withstand the heat load from 2 MW/m^2 up to 10 MW/m^2 in 2019. Equilibrium for this shot is provided by the equilibrium fitting (EFIT) code. The computational region includes the "core" region [a small segment of the region with closed field lines, i.e., the area between core edge interface (CEI) and separatrix], left SOL and right SOL regions, and the private flux regions (PFR), including upper and lower PFR. The grid has 100 poloidal including the guard cells at four targets and 38 radial cells including the guard cells at the core and SOL boundaries, with the separatrix being located between cell number 18 and 19. It stretches radially from about −3.8 cm to 3.7 cm on either side of the separatrix at the outer midplane.

B. Boundary conditions and modeling assumptions

In modeling, the multi-fluid species includes D^0 neutrals, D^+ main ions, and C impurities with neutral C^0 and all charged state ions and additional N^{0-7+}, Ne^{0-10+}, and Ar^{0-18+} in N, Ne, and Ar seeding cases, respectively. Carbon is produced self-consistently from physical and chemical sputtering and has zero recycling at targets, PFR, and SOL boundaries. The physical sputtering rates for both ions and neutrals are taken from the TRIM database.[16] Constant chemical sputtering rate 2% is used for carbon production. The hydrocarbons are not included in this paper. The sputtered material and the seeded impurities (N, Ne, and Ar) which are injected from the lower dome as shown in Fig. 1 are treated as atoms. The power across the CEI which enters into the computational region is set to $P_{CEI} = 1.6$ MW, which is calculated according to the energy balance by subtraction of ∼20% radiation power (=0.4 MW) inside the CEI surface not accounted in these simulations from the total heating power. It is equally distributed between electrons and ions. The electron density is set to $1.0 \times 10^{19}\,m^{-3}$ at the outer midplane separatrix and maintained by an automatic feedback loop through D_2 gas puffing outside the SOL region (see Fig. 1). Normally, the anomalous cross-field transport coefficients are determined by fitting the upstream density (n_e) and temperature (T_e) profiles measured by the Reciprocating Probe (RP) and edge Thomson Scattering (TS) system. However the upstream profiles for n_e and T_e are not available for this discharge, so we choose a typical empirical value for L-mode, $D_\perp = 0.3\ m^2s^{-1}$ and $\chi_e = \chi_i = 1.0\ m^2s^{-1}$ for particle and ion and electron heat diffusivities, respectively, in this paper. The parallel plasma transport is flux limited, and no drifts are included in this simulation. The radial temperature and density decay length, λ_T and λ_n, for SOL boundary are set to 0.03 m. The recycling coefficients for D^0 and D^+ are set to 1.0 at the PFR and outer SOL boundaries. At the divertor target plates, the sheath boundary condition is applied. According to the Bohm criterion, the flow will be at least the sonic speed at the sheath

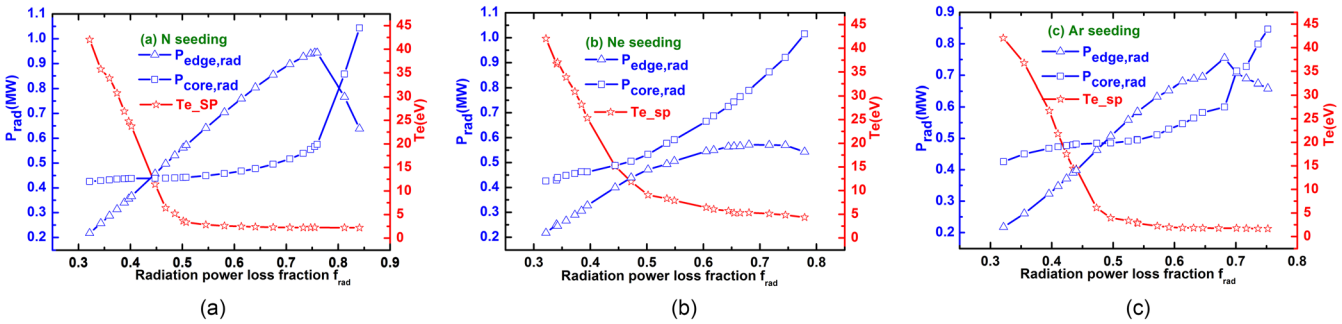

FIG. 2. The radiation in the edge (the whole area outside the separatrix) and in the core region (including the radiation inside CEI surface) and the electron temperature at the strike point of lower outer divertor against radiation power loss fraction for N (a), Ne (b), and Ar seeding (c) are shown.

entrance. The sheath heat transmission coefficients for electrons and ions are set to 4.5 and 2.5, respectively.

III. SIMULATION RESULTS AND DISCUSSIONS

A. The distribution of radiation power and its effect on divertor behavior

To investigate the distribution and its effect on the heat flux load and temperature at divertor targets with N, Ne, and Ar seeding in detail, we have carried out an impurity puffing rate scan. The radiation power in the edge region ($P_{edge,rad} = P_{SOL,rad} + P_{div,rad}$, i.e., the whole area outside the separatrix including SOL and divertor region) and in core region which covers the entire area inside separatrix surface ($P_{core,rad} = 0.4\,MW + P_{core,SOLPS}$, here 0.4 MW is ~20% radiation power inside the CEI surface not accounted in simulation and $P_{core,SOLPS}$ is the power radiated between CEI and separatrix calculated by SOLPS) and the electron temperature at the strike point of lower outer divertor as a function of radiation power loss fraction f_{rad} ($=P_{rad,tot}/P_{in}$) for N, Ne, and Ar seeding are shown in Figs. 2(a)–2(c), respectively, here $P_{rad,tot} = P_{core,rad} + P_{edge,rad}$. We can find that the highest radiative loss fraction (f_{rad}) for N seeding can reach ~85%, which is higher than Ne seeding of f_{rad} ~80% and Ar seeding of $f_{rad} \sim 75\%$. For N seeding, $P_{edge,rad}$ increases as f_{rad} increases and reaches the maximum value at $f_{rad} \sim 75\%$, while $P_{core,rad}$ is almost flat when $f_{rad} < 75\%$. When $f_{rad} > 75\%$, the radiation power inside separatrix increases dramatically and finally exceeds the edge radiative power at $f_{rad} \sim 80\%$. For Ar seeded case, both $P_{edge,rad}$ and $P_{core,rad}$ increase, and it increases faster in the edge region than in the core region when $f_{rad} < 65\%$, and the radiation in the core region dominates when $f_{rad} > 70\%$. For Ne case as shown in Fig. 2(b), $P_{core,rad}$ is completely above $P_{edge,rad}$ and $P_{core,rad}$ ramps up faster than $P_{edge,rad}$, which means that the radiation loss power induced by Ne is focused inside the separatrix for this shot. We also found that all of N, Ne, and Ar seeding can effectively reduce the peak electron temperature T_e and heat load (which has the same profiles with peak Te, so they are not shown in Fig. 2) at divertor targets similarly. The modeling results show that all divertor targets can get complete or partial detachment when the impurity gas puffing reaches a relatively high level of $f_{rad} \sim 60\%$.

To compare the loss power radiated in the core and edge region clearly, we plot the radiation power ratio of edge to core against f_{rad} with N, Ne, and Ar seeding in Fig. 3. As can be seen, the highest ratio is N seeding plasma, followed by Ar and Ne which has the lowest ratio, which is completely below 1. It suggests that $P_{core,rad}$ is higher for low-Z N seeding than Ne and Ar. It also can be found that for these three impurities the ratio increases against f_{rad} and reaches the maximum value, then drops. The maximum $P_{edge,rad}/P_{core,rad}$ reaches at $f_{rad} \sim 70\%$ for N, $f_{rad} \sim 50\%$ for Ne, and $f_{rad} \sim 60\%$ for Ar seeding. The ratio increases faster in N seeding plasma than in Ne and Ar cases. It indicates that when seeding with N, the increased radiative power is mainly in the edge region, while in the Ar case, power radiated in the core region is also significant. For the Ne case, more than 50% of radiation power is lost inside separatrix.

In fact, according to the radiation power formula $P_{rad} = n_e \sum_z n_z L_z$[17] with n_e and n_z being electron and impurity density and L_z being the radiative power loss rate, the different radiation power distributions among N, Ne, and Ar seeded plasma are in strong connection with their different radiation characteristics along the plasma temperature. Figure 4 shows L_z of some important elements in tokamak plasma as a function of temperature at a fixed n_e ($\sim 10^{20}\,m^{-3}$) calculated from the non-local thermodynamic equilibrium (NLTE) collisional radiative (CR) model by FLYCHK code.[18] We can see that the radiation peak of N is

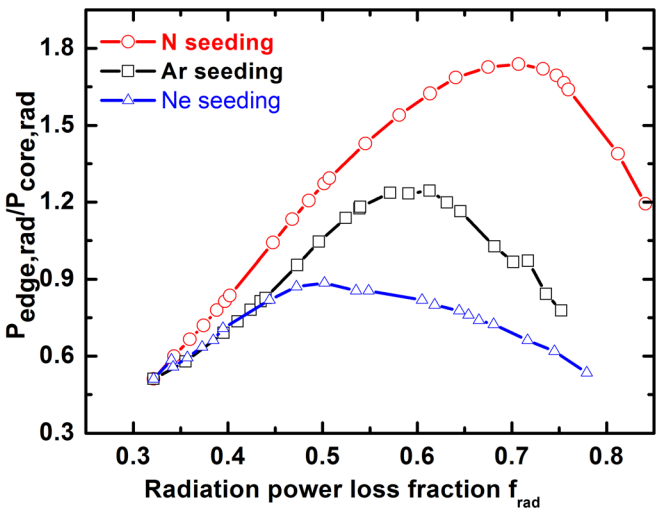

FIG. 3. The radiative power ratio of edge to core as a function of radiation power loss fraction with N, Ne, and Ar seeding.

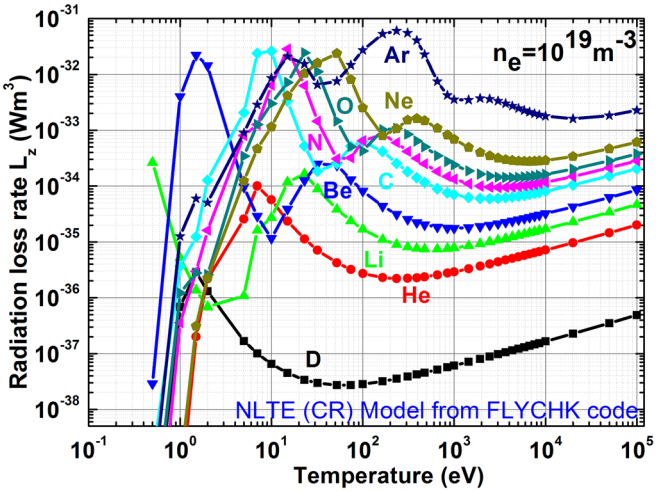

FIG. 4. The radiative power loss rate L_z of some important elements in tokamak as a function of temperature at a fixed n_e.

at Te ∼ 10–30 eV, which is the temperature typical in divertor, so N is a good divertor radiator for EAST. The first radiation peak of Ar is almost at the same Te with N, and there is another higher radiation peak at Te ∼ 100–500 eV. For Ne, the radiation peak is between the two peaks of Ar; it mainly radiates power at Te ∼ 20–80 eV, which is the temperature prevalent around the X-point and separatrix for this discharge.

In Fig. 5, we plot the total line radiation power for N, Ne, and Ar seeding cases at $f_{rad} \sim 60\%$. As can be seen, N and Ar seeding cases have the similar radiation loss power in the divertor region, but there is a remarkably larger radiation power inside separatrix for Ar seeding. In the Ne seeding case, as expected, the power is mainly radiated around the X-point and separatrix. The results suggest that N is a good radiator only for divertor, while Ar is a good for both the divertor and core region simultaneously; it may be suitable for ITER or CFETR to reduce the power entering into the SOL region and to enhance the radiation loss power in the divertor region. We also can find that N has the similar L_z with C; it seems to be a C-like radiator.

B. The effect of impurity seeding on P_{sep} and edge Z_{eff}

Besides the mitigation of divertor heat load, another crucial consideration for impurity seeding is the effect on core plasma performance. The effect of different impurities seeding on the energy confinement has been investigated on experiments.[8,9] The results show that normalized energy confinement factor H_{98} (an indicator of plasma confinement) is to a large degree independent of impurity when P_{sep} is larger than the threshold power of L-H mode transition (P_{th}), while N is better for the improvement of H_{98} than Ne and Ar when $P_{sep} < P_{th}$. It means that H_{98} depends strongly on the difference between input power and the radiative power inside the LCFS, P_{sep}. So, we plot P_{sep} with N, Ne, and Ar seeding against f_{rad} in Fig. 6. As we can see, P_{sep} decreases faster with Ne and Ar seeding than N. As it is shown in Fig. 5, Ne and Ar impurities have a larger radiation loss inside separatrix which results in the reduction of P_{sep}. So for the discharges with heating power being marginally over or around P_{th}, Ne and Ar seeding may induce the degradation of H_{98} and eventually trigger the back transition from the H- to L-mode. It should be noted that the P_{sep}, especially for Ne and Ar seeding cases, might be underestimated due to the assumption of the radiative power inside the CEI surface as a constant (∼0.4 MW). The P_{sep} in Ne and Ar seeding cases may decrease faster than we calculate. It indicates that Ne and Ar impurities are not good radiators when the power entering into SOL is very close to P_{th}, while they may be effective to reduce the power transported into the SOL region and be beneficial to lowering the heat load on divertor for high power discharges.

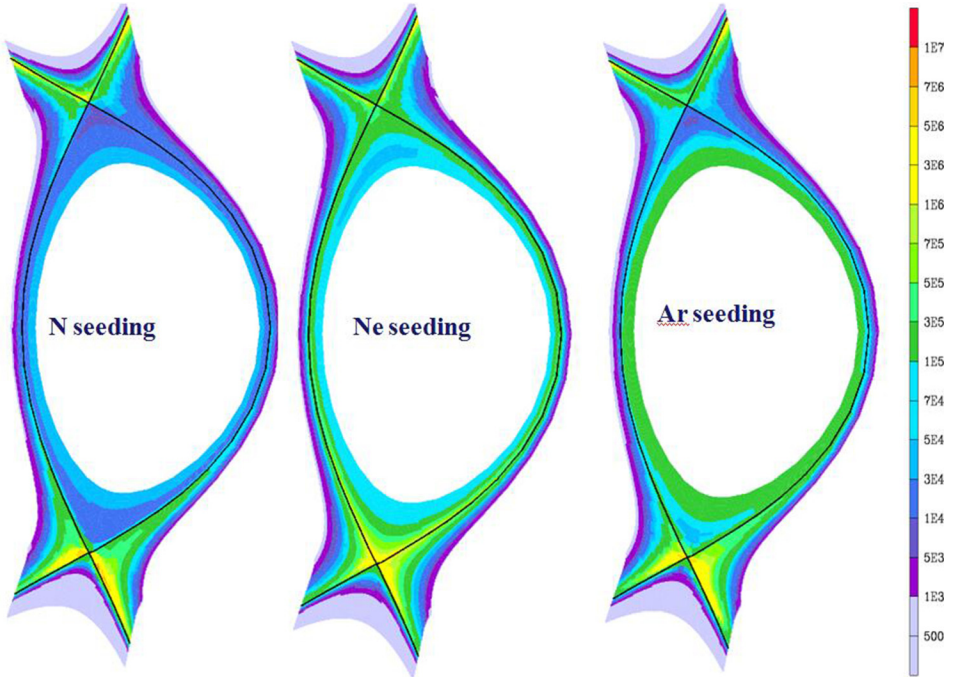

FIG. 5. The radiative power distribution (W/m^3) for N, Ne, and Ar seeding at the radiation power fraction $f_{rad} \sim 60\%$.

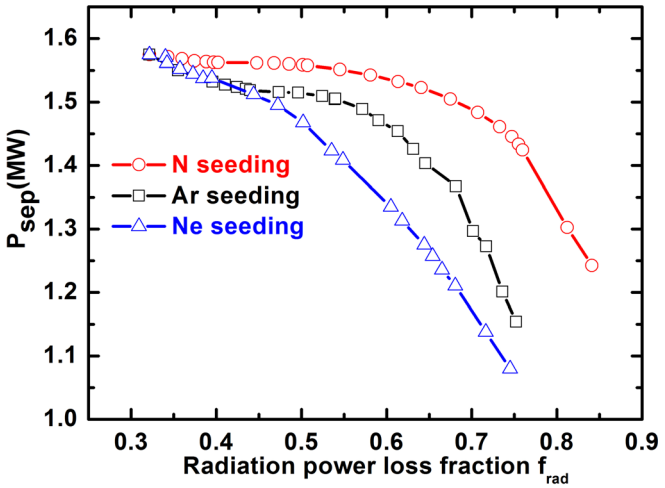

FIG. 6. The power across to separatrix (P_{sep}) is plotted as a function of radiation power loss fraction with N, Ne, and Ar seeding.

Another crucial detrimental effect of seeded impurities on the core plasma is the dilution of fuel particles. To minimize the negative effect on core plasma, impurities must be well confined in the divertor region with a minimal concentration in the core and SOL plasma. So a comparison of N, Ne, and Ar concentration in the SOL region along the poloidal length, from the outer midplane (OMP) to the outer strike point on divertor plate at a fixed radiation fraction, $f_{rad} \sim 60\%$, is plotted in Fig. 7. As can be seen, in SOL (i.e., from OMP to X-point), Ne has a higher concentration than those of N and Ar, while in the divertor region, especially near the target plate, N and Ar impurity concentration are almost 1.3–1.5 times as high as Ne impurity. The effective ion charge number, Z_{eff}, which also indicates the degree of plasma pollution, is of high interest in fusion plasma since the tolerable impurity level to achieve successful ignition is limited. However, a certain degree of dilution is of benefit to the edge temperature enhancement.[9,19] A correlation between the improvement of H_{98} and the increase in edge Z_{eff} was also found on ASDEX Upgrade.[9,19] The main reason is described as that impurity seeding allows a higher ion temperature at the same time edge ion pressure. This is caused by the reduction of ion temperature gradient (ITG) mode due to deuterium dilution induced by impurity seeding.[20] However, with a further increase in edge Z_{eff}, the radiative power inside the separatrix increases significantly which results in a significant decrease in P_{sep} to below the threshold power of H- to L-mode transition and thus the confinement eventually degrades as mentioned above. In Fig. 8, we plot Z_{eff} at the CEI surface at outer midplane as a function of f_{rad} with N, Ne, and Ar seeding. It is found that edge Z_{eff}, is totally larger in Ne seeding than in N and Ar seeding at a fixed f_{rad}. This is consistent with their concentration at OMP shown in Fig. 7. All of them increase significantly while $f_{rad} > 0.5$. Z_{eff} in N seeding case is a little larger than that in Ar injection case. It may mean that it has the best effectiveness of screening for Ar atom, followed by N and finally Ne atom. The effect of shielding of neutral impurities is mainly determined by the recycling, divertor geometry, and the mean free path for ionization which is actually determined by divertor parameters, like density and temperature.[4] Since the first two factors are the same for our simulations, it can be expected that the ionization mean free path λ_Z of impurity possibly plays a strong role in the divertor retention of these impurities. Impurities with bigger λ_Z will much more easily transport upstream or into core region. λ_Z can be expressed as a formula: $\lambda_z = v_i/(R_i n_e)$,[17] where v_i and R_i are the puffing velocity and the ionization rate coefficients for neutral impurities. Here, we assume that all impurities are puffed at room temperature ($\sim$300 K), and the thermal velocity is $\sqrt{2T/m_Z}$. Before impurity seeding, the electron density and temperature in divertor are really similar; in that case, the mean free path of ionization λ_Z for Ne is remarkably larger than N and Ar. Ar has the shortest λ_Z in the whole electron temperature at a typical divertor electron density $n_e = 5 \times 10^{19}\,m^{-3}$, as shown in Fig. 9. This may partially explain the concentration and Z_{eff} profiles shown in Figs. 7

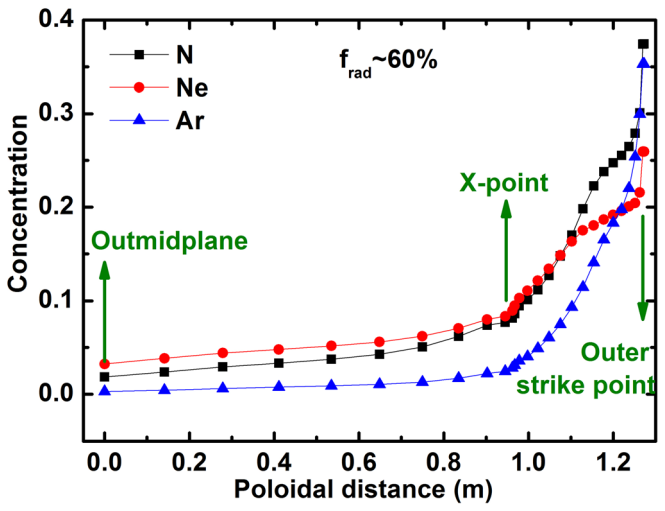

FIG. 7. The concentration of N, Ne, and Ar along the poloidal length from outer midplane to outboard strike point at the radiation power fraction $f_{rad} \sim 60\%$.

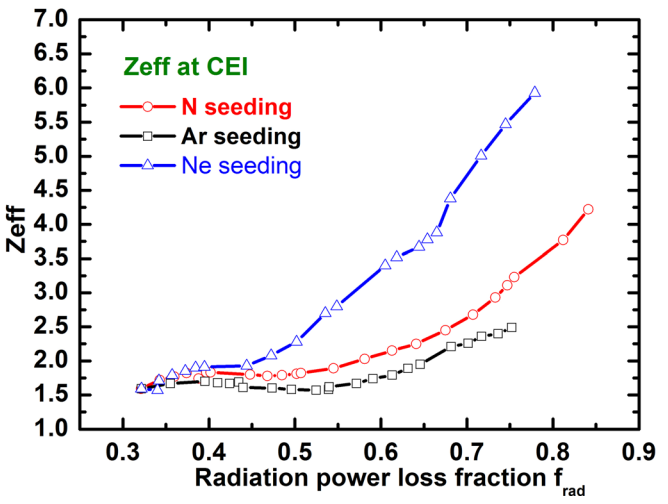

FIG. 8. The effective ion charge number at CEI against radiation power loss fraction with N, Ne, and Ar seeding.

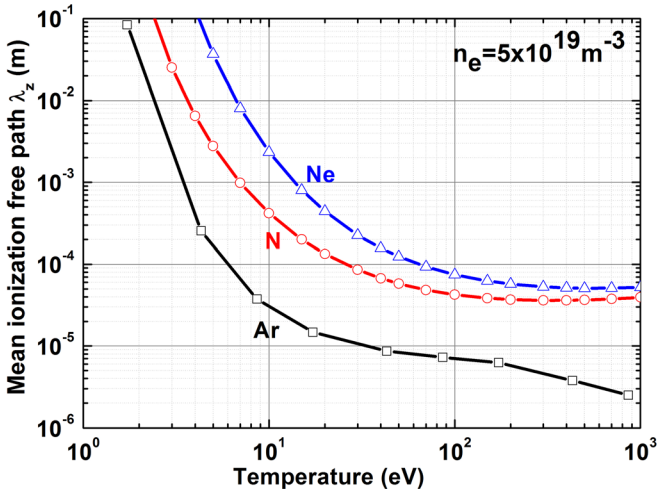

FIG. 9. The mean free ionization path of N, Ne, and Ar along with electron temperature at a typical divertor electron density $n_e = 5 \times 10^{19}\ m^{-3}$.

and 8. Another possible reason for the low edge Z_{eff} for Ar seeding plasma may be the low puffing rate of Ar. For a fixed f_{rad}, compared with N and Ne, Ar has a lower puffing rate due to its higher radiation loss rate. As we discussed above, in terms of fuel dilution, N and Ar impurities are more acceptable than Ne for this discharge. More detailed experimental validation on EAST will be performed in future.

IV. SUMMARY AND CONCLUSIONS

Radiative divertor discharges with N, Ne, and Ar seeding have been simulated by using SOLPS on EAST with double null configurations for L-mode discharge. The results indicate that N, Ne, and Ar seeding can effectively reduce the peak heat load and electron temperature Te on divertor targets similarly. The outer divertor gets detachment when the impurity puffing rate reaches a high level for all the three impurities. Additionally, the maximum radiation power loss fraction $f_{rad} \sim 85\%$ in N seeding is higher than in Ne and Ar seeding cases with $f_{rad} \sim 80\%$ and $f_{rad} \sim 75\%$, respectively. Both N and Ar have strong radiation power loss in the divertor region, while the radiative power inside separatrix for Ar seeding is also significant compared to N seeding case. Ne mainly radiates power around the X-point and a little inside separatrix. The radiation ratio of edge to core region increases before it decreases due to the radiation region moving into the separatrix as the impurity puffing rate increases. Furthermore, we have found that Ne and Ar impurities seeding results in a faster decrease of P_{sep} than that in N seeding case. The significant reduction of P_{sep} can eventually degrade the core performance of fusion plasma according to the discussion in Sec. III B. It suggests that Ne and Ar may be not good radiators for the heating power close to the L-H transition threshold. From the comparison of concentration in SOL along the poloidal length from OMP to the outer strike point and edge Z_{eff} with N, Ne, and Ar seeding, we can learn that Ne has a totally larger concentration at outer midplane and edge Z_{eff} than those in N and Ar seeding cases because Ne has a larger mean free ionization path which makes Ne escape more easily from divertor to the upstream. It suggests that N and Ar impurities are more acceptable than Ne in terms of fuel dilution for this discharge. It seems that N is well suited and better than Ne and Ar for EAST due to its high radiation loss power dominated in the divertor region and the low dilution level of main plasma.

In fact, not only do the electron temperature-dependent radiation characteristic and mean free ionization path of impurities play primary roles but also their transport in edge and divertor can be expected to be important in affecting the distribution of radiation loss power induced by impurities seeded. Further work on impurity transport with different transport coefficients and the effect of drifts will be performed in future.

ACKNOWLEDGMENTS

We would like to express our gratitude to D. Coster of IPP-Garching for the help in the application of the SOLPS code. Numerical computations were performed on the ShenMa High Performance Computing Cluster at the Institute of Plasma Physics, Chinese Academy of Sciences. This work was supported by the National Nature Science Foundation of China under Contract Nos. 11575236 and 11575244, National Magnetic Confinement Fusion Science Program of China under Contract Nos. 2014GB106005, 2014GB110003, 2015GB103002, and 2015GB103003, and the National Key Research and Development Program of China under Contract No. 2017YFA0402500.

[1]J. Li, H. Y. Guo, B. N. Wan, X. Z. Gong, Y. F. Liang, G. S. Xu, K. F. Gan, J. S. Hu, H. Q. Wang, L. Wang *et al.*, Nat. Phys. **9**(12), 817–821 (2013).
[2]Y. X. Wan, J. G. Li, Y. Liu, X. L. Wang, V. S. Chan, C. G. Chen, X. R. Duan, P. Fu, X. Gao, K. M. Feng *et al.*, Nucl. Fusion **57**, 102009 (2017).
[3]G. Janeschitz, A. Antipenkov, G. Federici, C. Ibbott, A. Kukushkin, P. Ladd, E. Martin, and R. Tivey, Nucl. Fusion **42**, 14 (2002).
[4]M. R. Wade, J. T. Hogan, S. L. Allen, N. H. Brooks, D. N. Hill, R. Maingi, M. J. Schaffer, J. G. Watkins, D. G. Whyte, R. D. Wood, and W. P. West, Nucl. Fusion **38**(12), 1839 (1998).
[5]W. P. West, N. H. Brooks, G. L. Jackson, A. W. Leonard, M. A. Mahdavi, T. H. Osborne, T. W. Petrie, M. J. Schaffer, R. D. Stambaugh, M. R. Wade *et al.*, J. Nucl. Mater. **266–269**, 44–50 (1999).
[6]H. S. Bosch, D. Coster, R. Dux, C. Fuchs, G. Haas, A. Herrmann, S. Hirsch, A. Kallenbach, J. Neuhauser, R. Schneider, J. Schweinzer, and M. Weinlich, J. Nucl. Mater. **241–243**, 82–91 (1997).
[7]J. A. Goetz, B. Lipschultz, C. S. Pitcher, J. L. Terry, P. T. Bonoli, J. E. Rice, and S. J. Wukitch, J. Nucl. Mater. **266–269**, 354–359 (1999).
[8]M. L. Reinke, J. W. Hughes, A. Loarte, D. Brunner, I. H. Hutchinson, B. LaBombard, J. Payne, and J. L. Terry, J. Nucl. Mater. **415**, S340 (2011).
[9]A. Loarte, J. W. Hughes, M. L. Reinke, J. L. Terry, B. LaBombard, D. Brunner, M. Greenwald, B. Lispschultz, Y. Ma, S. Wukitch, and S. Wolfe, Phys. Plasmas **18**, 056105 (2011).
[10]A. Kallenbach, M. Bernert, R. Dux, L. Casali, T. Eich, L. Giannone, A. Herrmann, R. McDermott, A. Mlynek, H. W. Müller *et al.*, Plasma Phys. Controlled Fusion **55**, 124041 (2013).
[11]M. Wischmeier, A. Huber, M. L. Reinke, C. Guillemaut, L. AhoMantila, S. Brezinesek, P. Drewelow, C. F. Maggi, K. McCormick, A. Meigs *et al.*, in *25th IAEA Conference, Saint Petersburg, Russia*, 13–18 October 2014.
[12]Z. S. Yang, J. B. Chen, D. P. Coster, Y. M. Duan, L. Wang, F. Ding, J. C. Xu, Q. Zang, T. F. Wang, N. Yan *et al.*, Phys. Plasmas **24**, 012503 (2017).
[13]R. Schneider, X. Bonnin, K. Borras, D. P. Coster, H. Kastelevicz, D. Reiter, V. A. Rozhansky, and B. J. Braams, Contrib. Plasma Phys. **46**(1-2), 3–191 (2006).

[14]D. Reiter, M. Baelmans, and P. Börner, Fusion Sci. Technol. **47**(2), 172–186 (2005).
[15]H. P. Summers, see http://www.adas.ac.uk./ for Atomic Data and Analysis Structure (ADAS) database, 2004.
[16]W. Echstein and D. B. Heifetz, J. Nucl. Mater. **145–147**, 332 (1987).
[17]M. Z. Tokar, Trans. Fusion Sci. Technol. **53**, 243 (2008).
[18]H.-K. Chung, see https://www-amdis.iaea.org/FLYCHK/ for NLTE kinetics modeling code.
[19]S. K. Rathgeber, R. Fischer, S. Fietz, A. Kallenbach, H. Meister, F. Ryter, G. Tardini, and E. Wolfrum, Plasma Phys. Controlled Fusion **52**, 095008 (2010).
[20]G. Tardini, R. M. McDermott, F. Jenko, T. Pütterich, S. K. Rathgeber, M. Schneller, J. Schweinzer, D. Told, and the ASDEX-Upgrade Team, in *37th EPS Conference on Plasma Physics, Sofia, Bulgaria*, 29 June–3 July, 2009.
[21]G. N. Luo, G. H. Liu, Q. Li, S. G. Qin, W. J. Wang, Y. L. Shi, C. Y. Xie, Z. M. Chen, M. Missirlian, D. Guilhem *et al.*, Nucl. Fusion **57**, 065001 (2017).